# Controlling the transport of single photons by tuning the frequency of either one or two cavities in an array of coupled cavities

Jie-Qiao Liao,[1,2] Z. R. Gong,[1,2] Lan Zhou,[3] Yu-xi Liu,[1,4] C. P. Sun,[1,2] and Franco Nori[1,5]

[1]*Advanced Science Institute, The Institute of Physical and Chemical Research (RIKEN), Wako-shi 351-0198, Japan*
[2]*Institute of Theoretical Physics, Chinese Academy of Sciences, Beijing 100190, China*
[3]*Key Laboratory of Low-Dimensional Quantum Structures and Quantum Control of Ministry of Education, Hunan Normal University, Changsha 410081, China and Department of Physics, Hunan Normal University, Changsha 410081, China*
[4]*Institute of Microelectronics, Tsinghua University, Beijing 100084, China*
[5]*Physics Department, The University of Michigan, Ann Arbor, MI 48109-1040, USA.*

(Dated: April 15, 2010)

We theoretically study how to control transport, bound states, and resonant states of a single photon in a one-dimensional coupled-cavity array. We find that the transport of a single photon in the cavity array can be controlled by tuning the frequency of either one or two cavities. If one of the cavities in the array has a tunable frequency, and its frequency is tuned to be larger (or smaller) than those of other cavities, then there is a photon bound state above (or below) the energy band of the coupled-cavity array. However, if two cavities in the array have tunable frequencies, then there exist both bound states and resonant states. If the frequencies of the two cavities are chosen to be much larger than those of other cavities, and the hopping couplings between any two nearest-neighbor cavities are weak, then a single photon with a resonant wave vector can be trapped in the region between the two frequency-tunable cavities. In this case, a quantum supercavity can be formed by these two frequency-tunable cavities. We also study how to apply this photon transport control to an array of coupled superconducting transmission line resonators.

PACS numbers: 03.67.Hk, 03.65.-w, 05.60.Gg



## I. INTRODUCTION

In a quantum network based on photons [1], the nodes can be regarded as information processing stations (e.g., quantum computers), while the links between any two nodes are provided by the information carriers (e.g., photons). Due to the high-speed transmission and low dissipation in optical fibers, photons are considered to be excellent information carriers (both for classical and quantum transmissions).

In recent years, with the development of nano-optics, numerous photonic information processing proposals have been implemented by using on-chip solid state devices, such as semiconducting microcavities (e.g., Ref. [2]) and superconducting transmission line resonators (e.g., Refs. [3–8]). Therefore, how to realize on-chip single-photon devices (e.g., Refs. [9–11]) becomes now an increasingly important research area. For example, single-photon switches (e.g., Refs. [12–16]), which control single-photon transport at will (e.g., Refs. [17, 18]), play an important role in this area.

Coupled-cavity arrays (CCAs) [19–30] are one type of photonic system, which has been proposed to process photonic quantum information. Compared with the usual waveguides, which have only a linear dispersion relation, the *nonlinear dispersion* of CCAs can result in the emergence of bound states of single photons. Many proposals have been put forward to realize quantum switches in CCAs, which could be used to control single-photon transport. For example, the reflection and transmission of single photons in a one-dimensional coupled resonator waveguide can be controlled by a tunable two-level system inside one of the cavities [14]. Moreover, controllable single-photon transport in a one-dimensional CCA with a tunable hopping coupling has recently been studied [16].

In this paper, we study another approach to realize controllable single-photon transport in a one-dimensional CCA, considering either one *frequency-tunable cavity* (FTC) or two FTCs. This work is motivated by recent mostly experimental results on frequency-tunable transmission line resonators (e.g., Refs. [31–37]), where the frequencies of the resonators can be changed by varying either the boundary condition of the electromagnetic wave or the magnetic flux through the SQUIDs used to construct the transmission line resonators. In contrast to Refs. [14, 27], here the photon transport is controlled by *tuning the frequency of the cavity*, and there is *no* additional two-level system, placed inside one of the cavities, to control photon transport. Therefore, this proposal seems to be simpler and easier to implement experimentally than those in Refs. [14, 27]. By changing the frequency of either one FTC or two FTCs, the reflection and transmission of a single photon in the coupled-cavity array can be controlled. We also study the photon bound states and photon resonant states [38] in this coupled-cavity array.

For the coupled-cavity array with *one* frequency-tunable cavity, if the frequency of the frequency-tunable cavity is larger than that of other cavities, there is a *bound* state above the energy band of the corresponding bosonic tight-binding model [39]; while the bound state is below the energy band when the frequency of the frequency-tunable cavity is smaller than that of other cavities.

For the CCA with *two* FTCs, we find that there exist *bound* states around the FTCs. Moreover, when the frequencies of the two FTCs are much larger than those of other cavities and the hopping couplings between any two nearest-neighbor cavities are weak, for resonant wave vectors, a single photon can be in resonance with the CCA and then remain trapped in the cavities between the two FTCs. A single photon in *resonance*

with the CCA behaves as a photon inside a supercavity [27].

This paper is organized as follows: In Sec. II, we study controllable single-photon transport and bound states in a CCA with one FTC. In Sec. III, we study controllable single-photon transport, bound states, and resonant states in the CCA with two FTCs. In Sec. IV, we present a possible experimental implementation of our proposal using superconducting transmission line resonators. A summary is given in Sec. V.

## II. COUPLED CAVITY ARRAY WITH ONE FREQUENCY-TUNABLE CAVITY

As schematically shown in Fig. 1, we consider a one-dimensional coupled-cavity array, which consists of a chain of $N$ cavities. We assume that $N$ is a large enough number, so periodic boundary conditions become reasonable. For specificity, and without loss of generality, we assume that $N$ is an odd number. The distance between any two nearest-neighbor cavities is $d_0$. The cavities, except the central one (i.e., the 0th cavity), have the same resonant frequency $\omega_c$. The central 0th cavity has the resonant frequency $(1+\lambda)\omega_c$, where $\lambda$ is used to characterize the detuning between the 0th cavity and other identical cavities, and assume to be varied for controlling the photon transport properties in this system. The frequency of the 0th cavity can be larger ($\lambda > 0$) or smaller ($\lambda < 0$) than those of other cavities. Any two nearest-neighbor cavities are coupled via a homogeneous hopping interaction of strength $J$. The Hamiltonian (with $\hbar = 1$) of the CCA reads

$$\hat{H}^{(1)}_{\rm CCA} = \lambda\omega_c\hat{a}_0^\dagger\hat{a}_0 + \sum_{j=-\frac{N-1}{2}}^{\frac{N-1}{2}} \omega_c\hat{a}_j^\dagger\hat{a}_j - \sum_{j=-\frac{N-1}{2}}^{\frac{N-1}{2}} J(\hat{a}_j^\dagger\hat{a}_{j+1} + \hat{a}_{j+1}^\dagger\hat{a}_j), \tag{1}$$

where $\hat{a}_j$ ($\hat{a}_j^\dagger$) is the annihilation (creation) operator of the $j$th cavity. The superscript "1" in $\hat{H}^{(1)}_{\rm CCA}$ denotes that the CCA contains one frequency-tunable cavity. The first two terms in Eq. (1) are the "free Hamiltonian" of the CCA, while the last term in Eq. (1) represents the hopping interaction, with strength $J$, between any two nearest-neighbor cavities. For instance, the term $\hat{a}_j^\dagger\hat{a}_{j+1}$ means that a photon is annihilated in the $(j+1)$th cavity and another photon is created in the $j$th cavity. Hereafter, we only use $\sum_j$ instead of the sum shown in Eq. (1). Since the frequency, $(1+\lambda)\omega_c$, of the 0th cavity should be nonnegative, then $\lambda \geq -1$. For $\lambda = 0$, the above Hamiltonian (1) reduces to the usual bosonic tight-binding (btb) Hamiltonian

$$\hat{H}_{\rm btb} = \omega_c\sum_j \hat{a}_j^\dagger\hat{a}_j - J\sum_j(\hat{a}_j^\dagger\hat{a}_{j+1} + \hat{a}_{j+1}^\dagger\hat{a}_j), \tag{2}$$

which can be diagonalized

$$\hat{H}_{\rm btb} = \sum_k \Omega_k\hat{a}_k^\dagger\hat{a}_k \tag{3}$$

by using the discrete Fourier transform

$$\hat{a}_k = \frac{1}{\sqrt{N}}\sum_j \exp(ikjd_0)\,\hat{a}_j \tag{4}$$

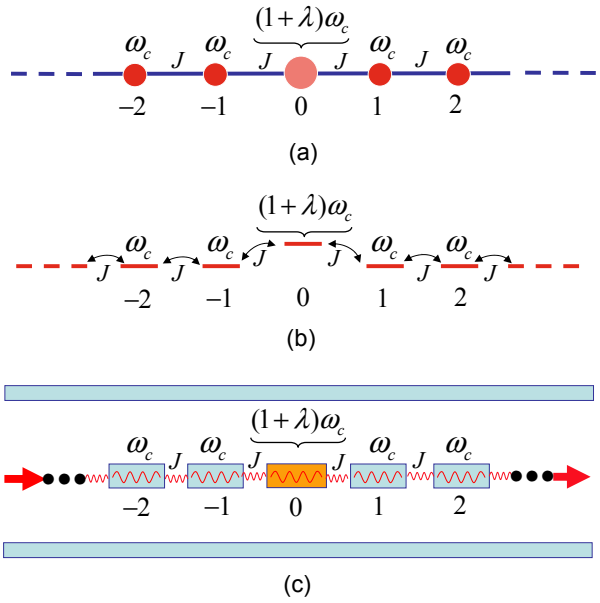


FIG. 1: (Color online) Schematic diagram of a one-dimensional coupled-cavity array (CCA): (a) a lattice model for the CCA. Each disk represents a cavity (labeled by the integer below each dot) with frequency shown right above each cavity. The larger disk (located at the site $j = 0$) represents the frequency-tunable cavity; (b) the energy levels of the CCA; (c) coupled superconducting transmission line resonator array. The central cavity located at the site $j = 0$ is shown in orange. This central cavity has a tunable frequency $(1+\lambda)\omega_c$, where $\lambda$ is the detuning parameter used to control the transport of single photons through this coupled-cavity array. If $\lambda > 0$ ($\lambda < 0$), then there is a photon bound state above (below) the energy band of the coupled-cavity array. Thus, the central cavity acts as a tunable "impurity". The arrows on the far left (right) schematically indicate the incoming (outgoing) photons. The blue dots represent the remaining cavities which are not shown here. The integers below each cavity label each one of them.

and the periodic boundary conditions, where

$$\Omega_k = \omega_c - 2J\cos(kd_0) \tag{5}$$

is a *nonlinear dispersion relation*, which is an energy band. Hereafter, the distance $d_0$ between two neighboring cavities is scaled as unity, and $k = 2\pi n_k/N$ (with $-N/2 < n_k \leq N/2$) are the photon wave vectors.

### A. Controllable single-photon transport for one frequency-tunable cavity

Since the total excitation number operator $\hat{N} \equiv \sum_j \hat{a}_j^\dagger\hat{a}_j$ of the CCA is a conserved observable, i.e., $[\hat{N}, \hat{H}^{(1)}_{\rm CCA}] = 0$, it is reasonable to restrict our discussions to the single-particle excitation subspace for studying single-photon transport. A general state in the single-excitation subspace can be written as

$$|\omega\rangle = \sum_j c_j|1_j\rangle, \tag{6}$$

where the state $|1_j\rangle = |0\rangle \otimes \cdots \otimes |1\rangle_j \otimes \cdots \otimes |0\rangle$ rep
the case when the $j$th cavity has one photon, while oth
ities have no photons. Also, $c_j$ is the probability ampli
the state $|1_j\rangle$. Using the discrete scattering method stu
Ref. [14] and the eigenequation $\hat{H}^{(1)}_{\rm CCA}|\omega\rangle = \omega|\omega\rangle$, we c

$$-J(c_{j+1} - c_{j-1}) = [\omega - (1 + \lambda\delta_{j0})\omega_c]c_j,$$

where $\delta_{j0}$ is the Kronecker delta function.

Without loss of generality, we assume that a single
with frequency $\omega = \Omega_k$ is injected from the left side
CCA, and then the photon probability amplitudes $c_j$
sumed to have the following solutions,

$$c_j = \begin{cases} e^{ikj} + re^{-ikj}, & j < 0, \\ se^{ikj}, & j > 0, \end{cases}$$

where $r$ and $s$ are the photon reflection and transmissi
plitudes, respectively. Here "$i$" denotes the imaginary u
cept when specified otherwise. It is easy to check that
is the solution of Eq. (7) when $j \neq 0$. Connecting Eq. (7) at
$j = 0$ with the continuity condition, $1 + r = s$, for the wave
function, we obtain the photon reflection amplitude

$$r = \frac{\lambda\omega_c}{2iJ\sin k - \lambda\omega_c}, \tag{9}$$

which leads to the photon reflection coefficient

$$R(k,\lambda) \equiv |r|^2 = \frac{(\lambda\omega_c)^2}{4J^2\sin^2 k + (\lambda\omega_c)^2}. \tag{10}$$

The reflection coefficient has three symmetric relations: $R(k,\lambda) = R(-k,\lambda)$, $R(\pi/2 - k,\lambda) = R(\pi/2 + k,\lambda)$, and $R(k,\lambda) = R(k,-\lambda)$. In Fig. 2, the reflection coefficient $R(k,\lambda)$, as a function of the detuning parameter $\lambda$, is plotted for $k = 0.01, \pi/8, \pi/4$, and $\pi/2$. It can be seen from Fig. 2 that the photon *reflection coefficient* $R(k,\lambda)$ *can be tuned* from zero to one by changing the detuning parameter $\lambda$.

### B. Bound states for one frequency-tunable cavity

A bound state may be formed when a particle is scattered by a localized potential. In the present model, the on-site extra energy $\lambda\omega_c$ acts as a potential. Therefore, a priori, this system may have bound states. First, we give a qualitative analysis of the bound states in the CCA. We now apply the discrete Fourier transform, defined in Eq. (4), to express the Hamiltonian (1) in wave vector space as follows,

$$\hat{H}^{(1)}_{\rm CCA} = \sum_k \Omega_k \hat{a}^\dagger_k \hat{a}_k + \frac{\lambda\omega_c}{N}\sum_{k,k'} \hat{a}^\dagger_k \hat{a}_{k'}. \tag{11}$$

In terms of the Hamiltonian in Eq. (11), we obtain the Heisenberg's equation of motion for the operator $\hat{a}_k$

$$i\dot{\hat{a}}_k = \Omega_k \hat{a}_k + \frac{\lambda\omega_c}{N}\sum_{k'} \hat{a}_{k'}. \tag{12}$$

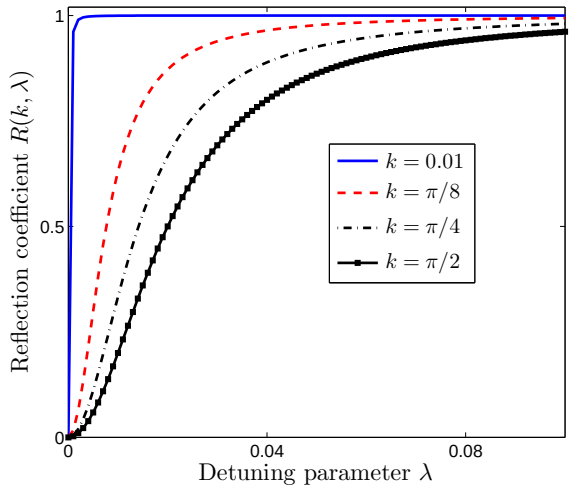


FIG. 2: (Color online) The photon reflection coefficient $R(k,\lambda)$ versus the detuning parameter $\lambda$ of the 0th cavity is plotted for $k = 0.01, \pi/8, \pi/4$ and $\pi/2$, where the parameters are taken in units of $\omega_c$, and $J/\omega_c = 0.01$. Recall that the on-site detuning of the central (0th) frequency-tunable cavity is $\lambda\omega_c$. A relatively small amount of detuning can make the reflection coefficient near one.

For small $\lambda$, we can assume that $i\dot{\hat{a}}_k = \omega_k\hat{a}_k$. By introducing the operator $\hat{b} \equiv \sum_k \hat{a}_k$, we obtain

$$\hat{a}_k = \frac{\lambda\omega_c}{N}\frac{1}{\omega_k - \Omega_k}\hat{b}. \tag{13}$$

Making the summation

$$\hat{b} = \sum_k \hat{a}_k = \frac{\lambda\omega_c}{N}\sum_k \frac{1}{\omega_k - \Omega_k}\hat{b}, \tag{14}$$

then the frequencies $\omega_k$ are determined by the equation

$$\frac{\lambda\omega_c}{N}\sum_k \frac{1}{\omega_k - \Omega_k} = 1. \tag{15}$$

Equation (15) can be solved numerically. In Figs. 3, the functions $f_1(\omega) = \lambda\omega_c\sum_k[1/(\omega - \Omega_k)]/N$ and $f_2(\omega) = 1$ are plotted for $\lambda > 0$ and $\lambda < 0$. The values of $\omega$ corresponding to the crossing points of both curves $f_1(\omega)$ and $f_2(\omega)$ are the solutions $\omega_k$ that satisfy Eq. (15). Obviously, when $\lambda > 0$ there is a bound state above the energy band, while for $\lambda < 0$ there is a bound state below the energy band. These bound states are shown as black circles in Fig. 3

Below, we analytically study the bound states. Since we choose the frequency-tunable cavity as the coordinate origin, the Hamiltonian (1) of the system is symmetric around the 0th cavity. The eigenstates of the Hamiltonian (1) have either symmetric or asymmetric parities. For the asymmetric case, we have the relation $c_j = -c_{-j}$, which implies $c_0 = 0$. Therefore, the frequency change of the frequency-tunable cavity will not affect the asymmetric eigenstates. For the symmetry case, we assume the following solution

$$c_j = A\,|\mu|^j, \tag{16}$$

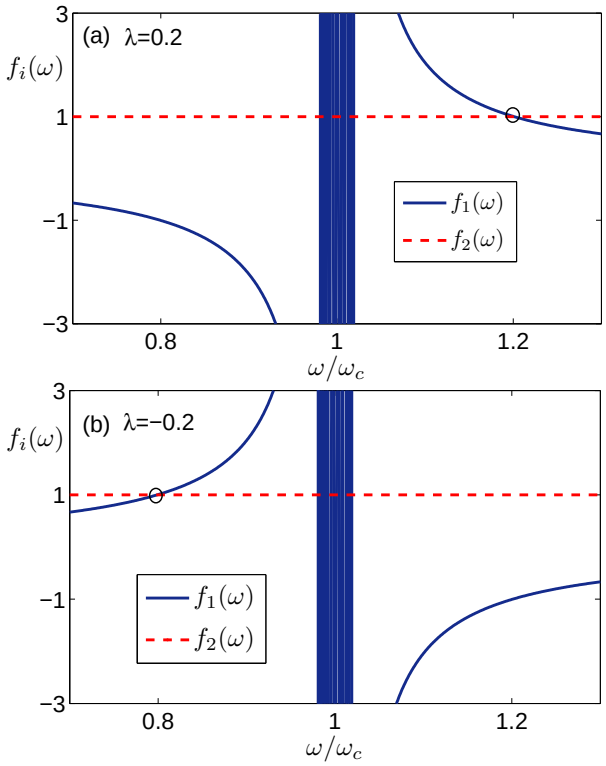


FIG. 3: (Color online) The functions $f_1(\omega) = \lambda\omega_c \sum_k [1/(\omega - \Omega_k)]/N$ (blue) and $f_2(\omega) = 1$ (red) versus the scaled frequency $\omega/\omega_c$. The values of $\omega$ corresponding to the crossing points between the curves for the functions $f_1(\omega)$ and $f_2(\omega)$ are the frequencies $\omega_k$. In other words, the $\omega_k$'s satisfy $f_1(\omega_k) = f_2(\omega_k)$. Here, the parameters are chosen as $N = 21$, $\omega_c = 1$, $J/\omega_c = 0.01$. Note that (a) and (b) use $\lambda = 0.2$ and $\lambda = -0.2$, respectively, and this is their only difference. Obviously, for $\lambda = 0.2$ ($\lambda = -0.2$), there is a bound state (shown as a black circle) above (below) the energy band ($0.98 < \omega/\omega_c < 1.02$).

where $\mu$ is a parameter introduced to describe the bound state of the Hamiltonian (1).

Substituting the solution (16) into Eq. (7), we obtain

$$-J\mu^2 + \lambda\omega_c\mu + J = 0. \tag{17}$$

Equation (17) has two solutions

$$\mu_\pm = \frac{-\lambda\omega_c \pm \sqrt{4J^2 + (\lambda\omega_c)^2}}{-2J}. \tag{18}$$

When $\lambda > 0$, we choose the solution $\mu_+$; while for the case $\lambda < 0$ we choose the solution $\mu_-$. The corresponding eigenfrequencies are

$$\omega_\pm = \omega_c \pm \sqrt{4J^2 + (\lambda\omega_c)^2}. \tag{19}$$

The relations $\omega_+ > \omega_c + 2J$ and $\omega_- < \omega_c - 2J$ mean that the bound state is above and below the energy band, respectively, as shown in Figs. 3(a) and 3(b). These analytical results are consistent with our previous analysis in Eqs. (11–15) and Fig. 3. Note that $\mu_+(|\lambda|) = -\mu_-(-|\lambda|)$, so $|c_j|^2$ is the same for the two bound states. In Fig. 4, we plot $|c_j|^2$ as a function

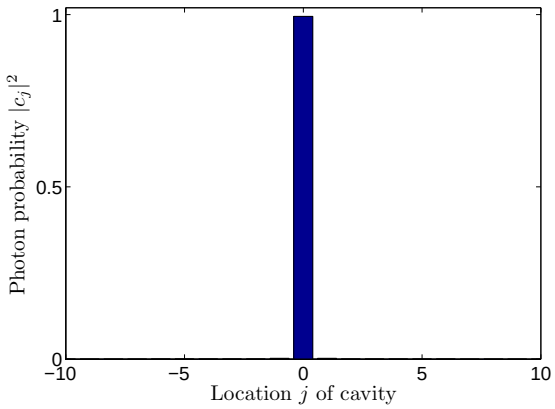


FIG. 4: (Color online) Photon probability $|c_j|^2$ versus the location $j$ of the cavity. The $c_j$'s are introduced in Eq. (6). Other parameters are taken as $\omega_c = 1$, $|\lambda| = 0.2$, and $J/\omega_c = 0.01$. In this case, since $|c_j|^2$ is peaked at the cavity located at $j = 0$, then *a single photon is localized* around the central (0th) frequency-tunable cavity.

of the lattice parameter $j$. Figure 4 shows that a single photon is mainly localized around the central (0th) frequency-tunable cavity.

### C. Links to localized excitations in solids

Periodic solid state systems exhibit bands. Adding localized defects to a translationally invariant structure induces localized states around those defects. In general, adding a defect (i.e., anything that breaks translational symmetry, like an impurity, or an interface) is enough to create gap states outside the continuous bands. Thus, gap states outside the bands are linked to localized states.

Figure 3 in this work is related to Fig. 9.9 in page 395 of Madelung's classic textbook [40] on solid state physics. Indeed, equation (9.37) in [40] is related to Eq. (15) in our paper. The links between them is that a defect added to a periodic structure tends to localize excitations around the defect, and this localized state corresponds to gap states.

## III. COUPLED CAVITY ARRAY WITH TWO FREQUENCY-TUNABLE CAVITIES

As schematically shown in Fig. 5, we now consider the case when there are *two* FTCs in the CCA. These two FTCs are located in the $-d$th and the $d$th cavities, respectively. The Hamiltonian can now be written as

$$\hat{H}^{(2)}_{\rm CCA} = \lambda_1\omega_c\hat{a}^\dagger_{-d}\hat{a}_{-d} + \lambda_2\omega_c\hat{a}^\dagger_d\hat{a}_d + \omega_c\sum_j \hat{a}^\dagger_j\hat{a}_j - J\sum_j(\hat{a}^\dagger_j\hat{a}_{j+1} + \hat{a}^\dagger_{j+1}\hat{a}_j), \tag{20}$$

where $\lambda_1$ and $\lambda_2$ are, respectively, used to describe the frequency of the $-d$th and the $d$th cavities, and $J$ is the hopping

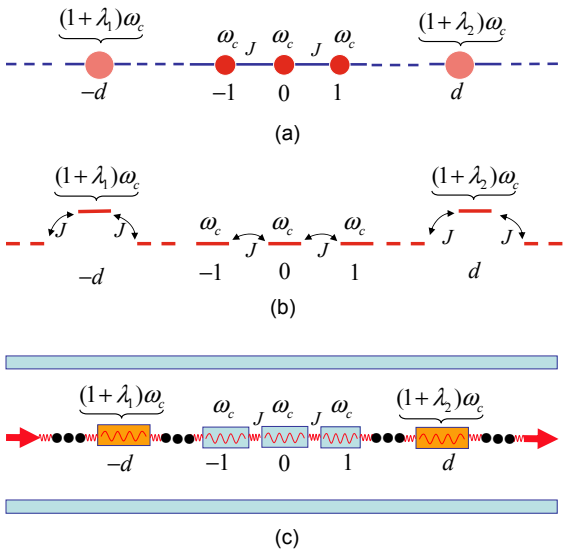


FIG. 5: (Color online) Schematic configuration of a one-dimensional coupled-cavity array with two frequency-tunable cavities: (a) a lattice model for the CCA. Each disk represents a cavity (labeled by the integer below each cavity) and with frequency shown right above it. The two larger disks (located at the sites $j = \pm d$) represent the two frequency-tunable cavities; (b) the energy levels of the CCA; (c) schematic diagram of a coupled superconducting transmission line resonator array. The two detuned cavities have frequencies $(1+\lambda_1)\omega_c$ and $(1+\lambda_2)\omega_c$. The two detuning parameters, $\lambda_1$ and $\lambda_2$, control the transport of single photons in the array of coupled cavities. The incoming photon can be localized at the cavities located at $j = \pm d$, forming localized bound states (in Fig. 8). Alternatively, when the photon wave vector is in resonance, the photon can be confined in the region between these two cavities, as shown in Fig. 9

coupling strength between any two nearest-neighbor cavities. The superscript "2" in $\hat{H}^{(2)}_{\rm CCA}$ means that the CCA contains two frequency-tunable cavities.

### A. Controllable single-photon transport for two frequency-tunable cavities

For the CCA with *two* frequency-tunable cavities, the total excitation number operator $\hat{N} \equiv \sum_j \hat{a}_j^\dagger \hat{a}_j$ is also a conserved observable. Similar to Eq. (6), the eigenstates of the system can now be written as $|\omega\rangle = \sum_j c_j |1_j\rangle$, where the coefficients $c_j$ are determined by the equation

$$-J(c_{j-1} + c_{j+1}) = \left[\omega - \omega_c\left(1 + \lambda_1\delta_{-d,j} + \lambda_2\delta_{d,j}\right)\right] c_j. \quad (21)$$

For simplicity, and without loss of generality, below we assume that the parameters for the two frequency-tunable cavities are identical, i.e., $\lambda_1 = \lambda_2 = \lambda_0$.

For a photon with frequency $\omega = \Omega_k$, the functions $\exp(ikj)$ and $\exp(-ikj)$ are the solutions of the Eq. (21) when $j \neq -d$ and $j \neq d$. Therefore, the general form of the solution for

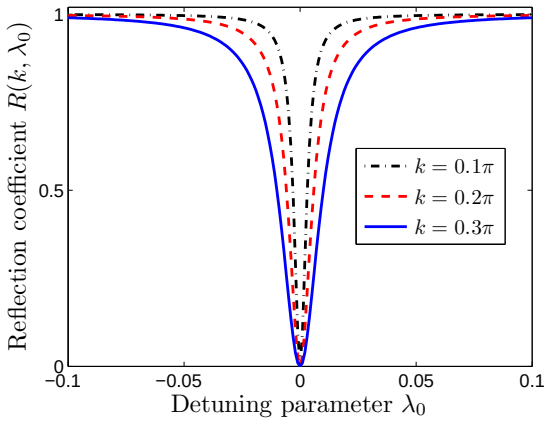


FIG. 6: (Color online) Photon reflection coefficient $R$ plotted versus the detuning parameter $\lambda_0$ for $k = 0.1\pi$, $0.2\pi$, and $0.3\pi$, where $\omega_c = 1$, $d = 5$, and $J/\omega_c = 0.01$. Here we consider two frequency-tunable cavities located at $j = -d$ and $j = d$. A relatively small amount of detuning can make the photon reflection coefficient near one.

Eq. (21) is assumed as

$$c_j = \begin{cases} e^{ikj} + re^{-ikj}, & j < -d, \\ Ae^{ikj} + Be^{-ikj}, & -d < j < d, \\ se^{ikj}, & j > d. \end{cases} \quad (22)$$

Substituting the solution (22) into Eq. (21) and using the continuity condition at $j = -d$ and $j = d$

$$e^{-ikd} + re^{ikd} = Ae^{-ikd} + Be^{ikd}, \quad (23a)$$
$$Ae^{ikd} + Be^{-ikd} = se^{ikd}, \quad (23b)$$

we obtain the photon reflection amplitude

$$\begin{aligned} r \;=\; & \lambda_0\omega_c e^{-i(2d-1)k}\left[J\left(1+e^{4ikd}\right)\left(e^{2ik}-1\right)\right. \\ & \left.+\lambda_0\omega_c\left(e^{4ikd}-1\right)e^{ik}\right] \\ & \times\left\{J\left(e^{2ik}-1\right)\left[J\left(e^{2ik}-1\right)-2\lambda_0\omega_c e^{ik}\right]\right. \\ & \left.-\lambda_0^2\omega_c^2\left(e^{4ikd}-1\right)e^{2ik}\right\}^{-1}. \end{aligned} \quad (24)$$

In Fig. 6, the photon reflection coefficient $R(k,\lambda_0) = |r|^2$ is plotted as a function of the parameter $\lambda_0$ for different wave vectors $k = 0.1\pi, 0.2\pi, 0.3\pi$. Figure 6 shows that the reflection coefficient $R(k,\lambda_0)$ can be tuned from zero to one by changing the detuning parameter $\lambda_0$.

### B. Bound states and resonant states for two frequency-tunable cavities

To study the bound states of the CCA with two frequency-tunable cavities, we assume

$$c_j = \begin{cases} Ae^{-ikj}, & j < -d, \\ Be^{ikj} + Ce^{-ikj}, & -d < j < d, \\ De^{ikj}, & j > d. \end{cases} \quad (25)$$

From Eq. (21) at $j = -d$, and the condition for the continuity of the wave function at $j = -d$, (namely: $Ae^{ikd} = Be^{-ikd} + Ce^{ikd}$), we obtain

$$\frac{A}{B} = \frac{i2J\sin k}{\lambda_0\omega_c}\exp(-2ikd), \tag{26a}$$

$$\frac{C}{B} = \frac{(i2J\sin k - \lambda_0\omega_c)}{\lambda_0\omega_c}\exp(-2ikd). \tag{26b}$$

From Eq. (21) at $j = d$, and the continuity condition at $j = d$, (that is $Be^{ikd} + Ce^{-ikd} = De^{ikd}$), we obtain

$$\frac{C}{B} = \frac{\lambda_0\omega_c}{i2J\sin k - \lambda_0\omega_c}\exp(2ikd), \tag{27a}$$

$$\frac{D}{B} = \frac{-i2J\sin k}{i2J\sin k - \lambda_0\omega_c}. \tag{27b}$$

Obviously, the right hand sides of Eqs. (26b) and (27a) should be equal; then we obtain

$$(\lambda_0\omega_c)^2\exp(4ikd) = (\lambda_0\omega_c - i2J\sin k)^2, \tag{28}$$

which implies

$$\exp(2ikd) = \pm\left(1 - \frac{i2J}{\lambda_0\omega_c}\sin k\right). \tag{29}$$

This Eq. (29) is important here because it determines the wave vector of the photon states (either bound states or resonant states). Below, we will discuss the existence of bound states in this system for the two cases shown in Eq. (29). These will be denoted as positive root and negative root, respectively, of Eq. (28). Also note that $\lambda_0$ takes two values ($\pm|\lambda_0|$) because the frequency detuning of the cavities at $j = \pm d$ can be either positive or negative.

### 1. *Positive root of Eq. (29)*

We now assume that the wave vector $k = x + iy$, with $y \geq 0$. It should be pointed out that the parameter $y$ can take the value $y = 0$ to include the possibility for the existence of some interesting resonant states. Since the energy of the photon must be a real parameter, (i.e., $\cos k = \cos x\cosh y - i\sin x\sinh y$ is real), this condition can be satisfied in the following three cases:

(1) $x = 2n\pi$, with $n \in Z$ (hereafter, $Z$ denotes the set of integers). In this case, $y$ is determined by the equation

$$\exp(-2dy) = 1 + \frac{2J}{\lambda_0\omega_c}\sinh y. \tag{30}$$

The solutions of the transcendent equation (30) (and other transcendent equations below) are determined through the numerical method briefly sketched in Fig. 7.

The coefficient relations in Eqs. (26) and (27) are

$$\frac{A}{B} = -\frac{D}{B} = \exp(2dy) - 1, \qquad \frac{C}{B} = -1. \tag{31}$$

When $\lambda_0 > 0$, from Fig. 7(a), we can see that Eq. (30) has only a "zero solution", $y = 0$, then $A = D = 0$ and $C = -B$, so

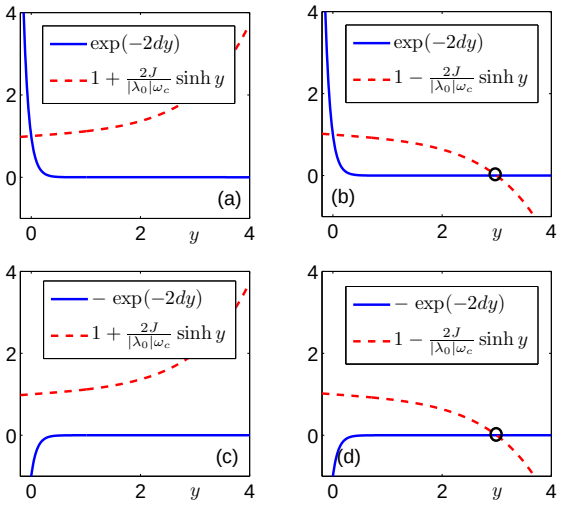


FIG. 7: (Color online) The functions $\exp(\pm 2dy)$ and $1 \pm 2J\sinh y/(|\lambda_0|\omega_c)$ are plotted as a function of $y$. The wave vector $k = x + iy$, with $y \geq 0$ here. The intersection points shown inside the black circles give the nonzero solutions of the transcendental equation (29). The parameters used here are $\omega_c = 1$, $J/\omega_c = 0.01$, $d = 5$, and $|\lambda_0| = 0.2$. Equation (29) determines the wave vector of the photon states (either bound states or resonant states).

the corresponding wave function $c_j = 0$. When $\lambda_0 < 0$, from Fig. 7(b), we know that Eq. (30) has two solutions: one is zero, and the other one is a positive number denoted by $y_0 > 0$. For the zero solution, the wave function is $c_j = 0$. For the solution $y_0 > 0$, we have $A = -D = (e^{2dy_0} - 1)B$ and $C = -B$. The corresponding wave function (25) becomes

$$c_j = \begin{cases} B(e^{2dy_0} - 1)e^{y_0 j}, & j < -d, \\ -2B\sinh(y_0 j), & -d < j < d, \\ -B(e^{2dy_0} - 1)e^{-y_0 j}, & j > d, \end{cases} \tag{32}$$

where $B$ is determined by the normalization condition. Obviously, the wave function (32) is asymmetric, i.e., $c_j = -c_{-j}$, so it is an odd-parity state. Using the parameters $\omega_c = 1$, $J/\omega_c = 0.01$, $d = 5$, and $|\lambda_0| = 0.2$, we obtain $y_0 = 2.998$. The photon probability corresponding to the wave function (32) is plotted in Fig. 8, which shows that the probability to find a single photon (32) is mostly around the two frequency-tunable cavities.

(2) $x = (2n + 1)\pi$, with $n \in Z$. In this case, $y$ is determined by the equation

$$\exp(-2dy) = 1 - \frac{2J}{\lambda_0\omega_c}\sinh y, \tag{33}$$

and the coefficient relations in Eqs. (26) and (27) are the same as those in Eq. (31). When $\lambda_0 < 0$, from Fig. 7(a), we can see that Eq. (33) has only a zero solution, $y = 0$, then $A = D = 0$ and $C = -B$. The corresponding wave function is $c_j = 0$. When $\lambda_0 > 0$, from Fig. 7(b), it can be seen that Eq. (33) has two solutions, one is zero, and the other is a positive number denoted by $y_0 > 0$. For the zero solution, the wave function is $c_j = 0$. For the solution $y_0 > 0$, then $A = -D = (e^{2dy_0} - 1)B$

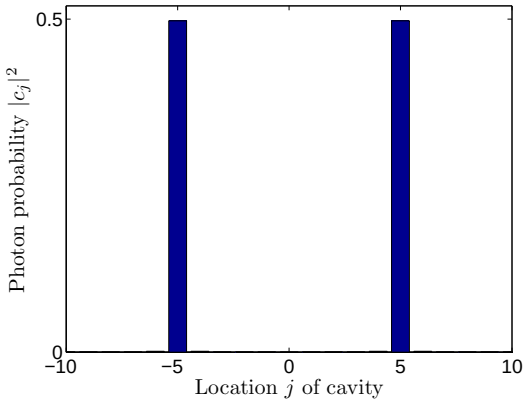


FIG. 8: (Color online) Photon probability $|c_j|^2$ of each coef of the normalized wave function given by Eqs. (6) and (32) parameters chosen here are $\omega_c = 1$, $J/\omega_c = 0.01$, $d = 5$, $y_0 =$ and with a detuning $|\lambda_0| = 0.2$ for the cavity at $j = \pm d$. The p is now localized and *bound at* the two detuned cavities loca $j = \pm d = \pm 5$.

and $C = -B$. The corresponding wave function becomes

$$c_j = \begin{cases} B(e^{2dy_0} - 1)e^{i(2n+1)\pi j}e^{y_0 j}, & j < -d, \\ -2Be^{i(2n+1)\pi j}\sinh(y_0 j), & -d < j < d, \\ -B(e^{2dy_0} - 1)e^{i(2n+1)\pi j}e^{-y_0 j}, & j > d. \end{cases} \quad (34)$$

The wave function in Eq. (34) is asymmetric for $j$, so it is an odd-parity state. The square of the module of the wave function in Eq. (34) is the same as that of the wave function in Eq. (32).

(3) $y = 0$. The motivation for studying the case $y = 0$ is to investigate whether there exist some interesting resonant states. In this case, $x$ is determined by the equation

$$\cos(2dx) = 1, \quad (35a)$$

$$-\frac{2J}{\lambda_0\omega_c}\sin x = 0. \quad (35b)$$

The solution of Eq. (35a) is $x = m\pi/d$, with $m \in Z$. For Eq. (35b), the solutions are $x = l\pi$, with $l \in Z$, for a general $2J/(\lambda_0\omega_c)$, or any $x$ when $\lambda_0\omega_c \gg 2J$, i.e., $2J/(\lambda_0\omega_c) \approx 0$. Connecting the solutions for the two Eqs. (35a) and (35b), we obtain two solutions for the case of $y = 0$: (a) $x = l\pi$, then the coefficient relations in Eqs. (26) and (27) become

$$\frac{A}{B} = \frac{D}{B} = 0, \qquad \frac{C}{B} = -1. \quad (36)$$

Therefore, the wave function is $c_j = 0$; (b) when $\lambda_0\omega \gg 2J$, in this case, we choose $x = m\pi/d$, then the coefficient relations in Eqs. (26) and (27) are the same as those in Eq. (36). The wave function becomes

$$c_j = \begin{cases} 0, & j < -d, \\ 2iB\sin\left(\frac{m\pi j}{d}\right), & -d < j < d, \\ 0, & j > d, \end{cases} \quad (37)$$

Obviously, the resonant state (37) is an odd-parity state with parameter $j$. The square of the module of the wave function in Eq. (37) is plotted in Fig. 9(a). We find that, when

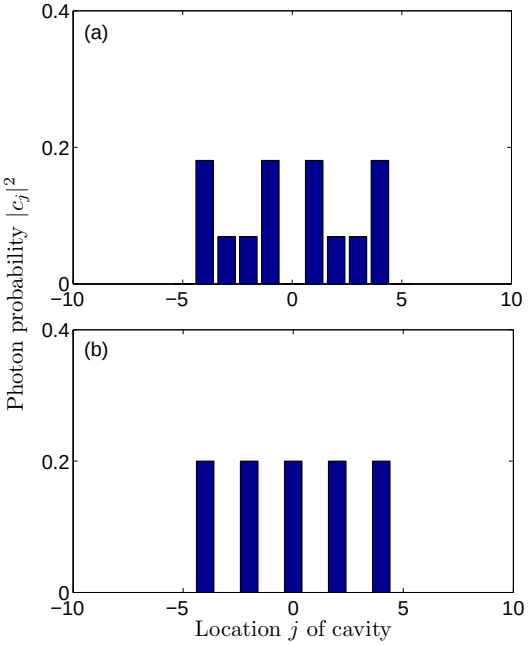


FIG. 9: (Color online) Photon probability $|c_j|^2$, given in Eqs. (37) and (45), versus the location $j$ of each cavity are plotted in figures (a) and (b), respectively. Here the parameters are set as $\omega_c = 1$, $m = 2$, $d = 5$, and $2J/(\lambda_0\omega_c) \approx 0$. Now the photon is *not bound at* $j = \pm d$, as in Fig. 8, but it is *confined in between* $j = \pm d = \pm 5$. This is because a single photon with wave vector (a) $2\pi/5$ and (b) $\pi/2$ is *in resonance* with the coupled-cavity array between the two detuned cavities located at $j = \pm d = \pm 5$. These are resonant states.

$\lambda_0\omega_c \gg 2J$, (i.e., the frequencies of the $-d$th and $d$th cavities are very largely detuned from those of other cavities and the hopping coupling $J$ between two nearest-neighbor cavities is weak), the photon with wave vector $m\pi/d$ ($m \in Z$) can produce a *resonance* in the region between the two FTCs, once it is injected there. Therefore, this resonant photon state is confined between the two cavities located at $j = \pm d$, as shown in Fig. 9(a).

### 2. *Negative root of Eq. (29)*

We now write the wave vector as $k = x + iy$, with $y \geq 0$. Since the energy of the photon must be real, (i.e., $\cos k = \cos x\cosh y - i\sin x\sinh y$ should be real), this condition can be satisfied in the following three cases:

(1) $x = 2n\pi$. In this case, $y$ is determined by the equation

$$-\exp(-2dy) = 1 + \frac{2J}{\lambda_0\omega_c}\sinh y, \quad (38)$$

and the coefficient relations in Eqs. (26) and (27) become

$$\frac{A}{B} = \frac{D}{B} = e^{2dy} + 1, \qquad \frac{C}{B} = 1. \quad (39)$$

In this case, when $\lambda_0 > 0$, we know from Fig. 7(c) that Eq. (38) has no positive solution. When $\lambda_0 < 0$, from

Fig. 7(d), we know that Eq. (38) has a positive solution $y_1$. Then $A = D = (e^{2dy_1} + 1)B$ and $C = B$. Therefore, the w function becomes

$$c_j = \begin{cases} B(e^{2dy_1} + 1)e^{y_1 j}, & j < -d, \\ 2B\cosh(y_1 j), & -d < j < d, \\ B(e^{2dy_1} + 1)e^{-y_1 j}, & j > d. \end{cases}$$

The wave function in Eq. (40) is an even-parity state. U the parameters $\omega_c = 1$, $J/\omega_c = 0.01$, $d = 5$, and $|\lambda_0| = 0.2$ obtain $y_1 = 2.998$. We found that the difference betwee and $y_1$ is very small, on the order of $10^{-12}$. Thus the ph probability $|c_j|^2$ here looks like the one in Fig. 8.

(2) $x = (2n + 1)\pi$. In this case, $y$ is determined by equation

$$-\exp(-2dy) = 1 - \frac{2J}{\lambda_0\omega_c}\sinh y,$$

and the coefficient relations in Eqs. (26) and (27) are the s as those in Eq. (39). When $\lambda_0 < 0$, from Fig. 7(c), we can that the Eq. (41) has no positive solution. When $\lambda_0 > 0$, f Fig. 7(d), we know that Eq. (41) has one positive solutio Then $A = D = (e^{2dy_1} + 1)B$ and $C = B$. So the correspon wave function now becomes

$$c_j = \begin{cases} B(e^{2dy_1} + 1)e^{i(2n+1)\pi j}e^{y_1 j}, & j < -d, \\ 2Be^{i(2n+1)\pi j}\cosh(y_1 j), & -d < j < d, \\ B(e^{2dy_1} + 1)e^{i(2n+1)\pi j}e^{-y_1 j}, & j > d, \end{cases}$$

This wave function (42) is an even-parity state. The squar the module of the wave function in Eq. (42) is the same as of the wave function in Eq. (40).

(3) $y = 0$. In this case, $x$ is determined by the equation

$$\cos(2dx) = -1, \tag{43a}$$

$$\frac{2J}{\lambda_0\omega_c}\sin x = 0. \tag{43b}$$

The solutions of Eq. (43a) are $x = (2m + 1)\pi/(2d)$, and the solutions of Eq. (43b) are $x = l\pi$ or any $x$ when $\lambda_0\omega_c \gg 2J$. Therefore, the solutions meeting the two equations (43a) and (43b) at the same time are $x = (2m + 1)\pi/(2d)$, when $\lambda_0\omega_c \gg 2J$. Then the coefficient relations in Eqs. (26) and (27) become

$$\frac{A}{B} = \frac{D}{B} = 0, \qquad \frac{C}{B} = 1. \tag{44}$$

Therefore, the wave function now becomes

$$c_j = \begin{cases} 0, & j < -d, \\ 2B\cos\left(\frac{(2m+1)\pi j}{2d}\right), & -d < j < d, \\ 0, & j > d. \end{cases} \tag{45}$$

This resonant state (45) is an even-parity state. The square of the module of the wave function (45) is plotted in Fig. 9(b). This figure shows that a single photon with wave vectors $(2m + 1)\pi/(2d)$ can be in resonance in the region between the two frequency-tunable cavities. For the two cases of resonant states given in Eqs. (37) and (45), the center cavities between the two frequency-tunable cavities form a supercavity [27]. We note that our approach is also valid for the case $\lambda_1 \neq \lambda_2$.

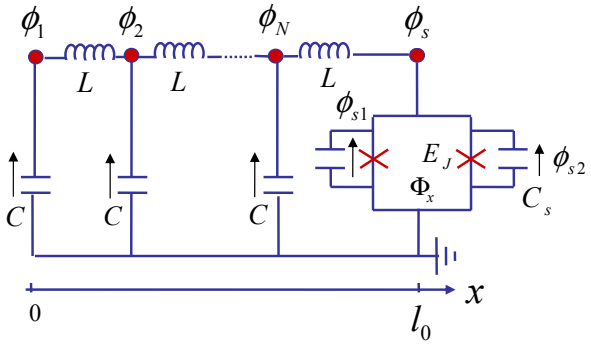


FIG. 10: (Color online) Circuit model of a frequency-tunable transmission line resonator integrated with a SQUID [31].

## IV. PHYSICAL REALIZATION OF FREQUENCY-TUNABLE SUPERCONDUCTING TRANSMISSION LINE RESONATORS

In this section, we study several physical realizations of a frequency-tunable coupled-cavity array by using superconducting transmission line resonators. In recent years, there have been several theoretical proposals and experiments on how to realize a frequency-tunable transmission line resonator (e.g., Refs. [31–37]).

Typically, there are two physical mechanisms to tune the resonant frequency of a superconducting transmission line resonator. One method is to change the boundary condition of the electromagnetic wave in a transmission line. By changing the boundary condition, the effective wavelengths (also effective frequencies) of the resonant modes are changed [31–33].

Another method is to construct a transmission line resonator by using a series of magnetic-flux-biased SQUIDs. Since the effective inductor of a magnetic-flux-biased SQUID can be tuned by changing the biased magnetic flux [34–36], the inductance per unit length of the SQUID array is controllable. Therefore, the resonant frequencies of the modes in the SQUID array can be tuned by controlling the biased magnetic flux threading through the SQUIDs.

Below, we present a brief review of these two methods already used to obtain frequency-tunable transmission line resonator. The original derivations of the two methods have been given in Refs. [31, 35], but for the sake of completeness of this paper, here we briefly review the main aspects of these.

### A. Tuning the frequency of a superconducting transmission line resonator: changing the boundary condition

We briefly summarize the mechanism for frequency tunability of a superconducting transmission line resonator by controlling its boundary condition [31]. The lumped element circuit of a superconducting transmission line resonator with a symmetric SQUID, which is equivalent to a chain of identical $LC$ circuits, is shown in Fig. 10. Here, $\phi_j$ is the phase variable of the $j$th node; $C$ and $L$ are respectively the capacitance and inductance of each $LC$ circuit; $\phi_{s1}$ and $\phi_{s2}$ are the phase

variables across the left and right Josephson junctions in SQUID, respectively; $C_s$ is the capacitance of one junctio the SQUID. The SQUID is equivalent to a junction with effective Josephson energy $E_J(f) = 2E_J\cos(f/2)$. Here $E$ the Josephson energy of one junction, $f = 2\pi\Phi_x/\Phi_0$, wh $\Phi_x$ is the flux through the loop of the SQUID and $\Phi_0$ is magnetic flux quanta. $\phi_s = (\phi_{s1} + \phi_{s2})/2$ is the net ph across the SQUID. Note that here the self-inductance of superconducting loop is neglected. When $\phi_s \ll 1$, and charging energy and Josephson energy satisfy the condit $E_J(f) \gg C_s[\Phi_0/(2\pi)]^2$, then the SQUID can be approxima as a harmonic oscillator [31]. For the phase variable of transmission line resonator, the wave equation reads [31]

$$\ddot{\phi}(x,t) - v^2\phi''(x,t) = 0, \qquad (46)$$

where $v = 1/\sqrt{C_0L_0}$. Here $C_0$ and $L_0$ are, respectively, capacitance and inductance per unit length of the transn sion line resonator; and $\phi''$ refers to the second-order spa derivative. Note that here we have used the continuous v able $x$ instead of the discrete variable $j$.

In terms of the relation between the electric current and phase $I(x,t) = -\Phi_0\phi'(x,t)/(2\pi L_0)$, the boundary condit for this system is [31]

$$I(0,t) = 0, \qquad \phi(l_0,t) = \phi_s(t), \qquad (47)$$

where $l_0$ is the length of the transmission line onator. The wave equation (46) with the boundary cor tion (47) can be solved by assuming the solution $\phi(x,t)$ $[A_1\cos(kvt) + A_2\sin(kvt)]\cos(kx)$. The Euler-Lagrange equation for the phase variable $\phi_s$ leads to the following dispersion equation [31]

$$kl_0\tan(kl_0) = \left(\frac{2\pi}{\Phi_0}\right)^2 E_J(f)\,L_{\rm cav} - \frac{2C_s}{C_{\rm cav}}k^2l_0^2, \qquad (48)$$

where $L_{\rm cav} = L_0l_0$ and $C_{\rm cav} = C_0l_0$. The wave vectors $k$ of the resonant modes in the transmission line resonator are the solutions of the dispersion equation (48). Since the effective Josephson energy $E_J(f)$ of the SQUID is tunable through the bias magnetic flux $\Phi_x$, the wave vectors $k$ can be tuned continuously by controlling $\Phi_x$. This approach [31] to tune cavities could be used to tune the frequency of either one cavity or two cavities in our proposal.

### B. Tuning the frequency of a superconducting transmission line resonator: changing the effective inductance of a SQUID

Following Ref. [35], Figure 11(a) shows a device where the center of the resonator is composed of a series array of SQUIDs. A symmetric SQUID (in Fig. 11(b)) is equivalent to an effective tunable inductance (shown in Fig. 11(c)). From Kirchhoff's current law and the Josephson current-phase relation [35], then

$$I = I_c\sin\phi_1 + I_c\sin\phi_2, \qquad (49)$$

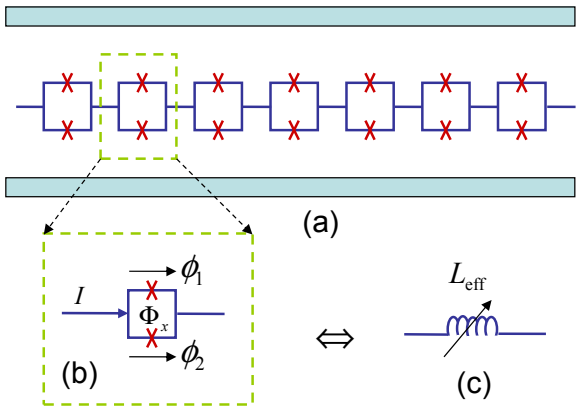


FIG. 11: (Color online) (a) Circuit model of a series array of SQUIDs. (b) Circuit model of a SQUID, which is equivalent to an effective tunable inductor in (c).

where $I_c$ is the critical current of a single Josephson junction, $\phi_j$ $(j = 1,2)$ are the phases across the two Josephson junctions. Introducing new phase variables $\phi = (\phi_1 + \phi_2)/2$ and $\phi_1 - \phi_2 = \phi_x$, then $I = I_c(\phi_x)\sin\phi$, where $I_c(\phi_x) = 2I_c\cos(\phi_x/2)$. The phase can be expressed as $\phi = \arcsin[I/I_c(\phi_x)]$. An effective inductance $L_{\rm eff}$ can be defined [35] by the phase $\phi$ and current $I$,

$$L_{\rm eff} = \frac{\Phi_0\phi}{2\pi I}, \qquad (50)$$

which can be expressed as [35]

$$L_{\rm eff}(I,\phi_x) = \frac{\Phi_0}{2\pi I}\arcsin\left(\frac{I}{I_c(\phi_x)}\right). \qquad (51)$$

Obviously, the effective inductance of the symmetric SQUID can be controlled through two externally controllable parameters: the biasing current $I$ and the external biasing flux $\Phi_x = \Phi_0\phi_x/(2\pi)$. Thus the resonant frequency of the modes in a SQUID array becomes tunable because the inductance per unit length of the center conductor of the transmission line resonator is controllable. This approach [35] could also be used to tune the frequency of either one cavity or two cavities in our proposed system. This would allow the exploration of the effect predicted here.

### C. Experimental implementation of our proposal

Let us now provide some remarks on the experimental implementation of our proposal. In our model, the key elements are the frequency-tunable cavities, which have recently been realized experimentally. For example, in Ref. [32], the resonant frequency $\omega_c$ of a transmission line resonator was tuned from $2\pi\times4$ GHz to $2\pi\times4.8$ GHz (i.e., $0 \le |\lambda\omega_c| \le 2\pi\times800$ MHz). If we choose $\omega_c \approx 2\pi\times4$ GHz, then $0 \le \lambda \le 0.2$, if we choose $\omega_c \approx 2\pi\times4.8$ GHz, then $-0.2 \le \lambda \le 0$. Similarly for $\lambda_0$. In principle, the hopping coupling $J$ between two nearest-neighbor transmission line resonators can be tuned [16]. In

recent experiments (e.g., in Ref. [41]), the magnitude of the hopping interaction is $J \approx 2\pi \times 44$ MHz $\approx 0.01\omega_c$. This hopping coupling $J$ can be increased by using larger capacitors to connect two transmission line resonators. Therefore, this study seems to be within the reach of current (or near future) experiments.

Compared to the method using a two-level atom as a controller, in Refs. [14, 27], the present proposal avoids photon dissipation due to the spontaneous emission of the atom.

It should be pointed out that we have neglected the change of the hopping coupling $J$ between the frequency-tunable cavity and its nearest-neighbor cavities when the frequency of the FTC is tuned. In practice, this dependence exists.

## V. SUMMARY

In conclusion, we have studied controllable single-photon transport and single-photon states in a one-dimensional coupled-cavity array (CCA) with one or two frequency-tunable cavities (FTCs). We found that, by adjusting the frequency of the frequency-tunable cavities, the coherent transport of a single photon in the CCA can be realized. We have also shown that there exist bound states in the CCA.

For a CCA with *one* FTC, when the frequency of the FTC is larger than those of other cavities, there exists a *bound* state above the energy band of the CCA. When the frequency of the FTC is smaller than those of other cavities, there exists a bound state below the energy band. In these two cases, the bound states have even parity. Once the frequency of the FTC is given, the CCA has only one bound state. This result is different from that of a CCA coupled with a two-level atom [14, 27], in which there exists two bound states at the same time, one above the energy band and the other below the energy band.

For a CCA with *two* FTCs, in the two cases that the frequencies of the two FTCs are larger or lower than those of other cavities, there exist two *bound* states, one of odd parity and the other one of even parity. When the frequency detuning $\lambda_0\omega_c$ of the two FTCs is very larger than the hopping coupling $J$ between two nearest-neighbor cavities, there exist two kinds of *resonant* modes, one of odd parity, and another one of even parity.

### Acknowledgments

This work is supported in part by NSFC Grants No. 10935010 and No. 10704023, NFRPC Grants No. 2006CB921205, No. 2007CB925204, and NCET-08-0682. Y. X. Liu is supported by NSFC Grants No. 10975080 and No. 60836001. F.N. acknowledges partial support from the National Security Agency, Laboratory Physical Science, Army Research Office, National Science Foundation Grant No. 0726909, and JSPS-RFBR Contract No. 06-02-91200.

[1] H. J. Kimble, Nature (London) **453**, 1023 (2008).
[2] K. J. Vahala, Nature (London) **424**, 839 (2003).
[3] J. Q. You and F. Nori, Phys. Today **58** (11), 42 (2005).
[4] R. J. Schoelkopf and S. M. Girvin, Nature (London) **451**, 664 (2008).
[5] G. Wendin and V. S. Shumeiko, in *Handbook of Theoretical and Computational Nanotechnology*, edited by M. Rieth and W. Schommers (American Scientific, New York, 2006) Vol. 3.
[6] A. Wallraff, D. I. Schuster, A. Blais, L. Frunzio, R. S. Huang, J. Majer, S. Kumar, S. M. Girvin, and R. J. Schoelkopf, Nature (London) **431**, 162 (2004).
[7] A. L. Rakhmanov, A. M. Zagoskin, S. Savel'ev, F. Nori, Phys. Rev. B **77**, 144507 (2008).
[8] D. I. Tsomokos, S. Ashhab, F. Nori, New J. Phys **10**, 113020 (2008).
[9] A. V. Akimov, A. Mukherjee, C. L. Yu, D. E. Chang, A. S. Zibrov, P. R. Hemmer, H. Park, M. D. Lukin, Nature (London) **450**, 402 (2007).
[10] Y. X. Liu, L. F. Wei, and F. Nori, Europhys. Lett. **67**, 941 (2004); Phys. Rev. A **71**, 063820 (2005); Phys. Rev. A **72**, 033818 (2005).
[11] J. Q. You, Y. X. Liu, C. P. Sun, and F. Nori, Phys. Rev. B **75**, 104516 (2007).
[12] C. P. Sun, L. F. Wei, Y. X. Liu, and F. Nori, Phys. Rev. A **73**, 022318 (2006).
[13] M. Mariantoni, F. Deppe, A. Marx, R. Gross, F. K. Wilhelm, and E. Solano, Phys. Rev. B **78**, 104508 (2008).
[14] L. Zhou, Z. R. Gong, Y. X. Liu, C. P. Sun, and F. Nori, Phys. Rev. Lett. **101**, 100501 (2008).
[15] Z. R. Gong, H. Ian, L. Zhou, and C. P. Sun, Phys. Rev. A **78**, 053806 (2008).
[16] J. Q. Liao, J. F. Huang, Y. X. Liu, L. M. Kuang, and C. P. Sun, Phys. Rev. A **80**, 014301 (2009).
[17] D. E. Chang, A. S. Sørensen, E. A. Demler, and M. D. Lukin, Nat. Phys. **3**, 807 (2007).
[18] J. T. Shen and S. Fan, Phys. Rev. Lett. **95**, 213001 (2005); **98**, 153003 (2007); Phys. Rev. A **79**, 023837(2009); **79**, 023838 (2009).
[19] M. J. Hartmann, F. G. S. L. Brandao, and M. B. Plenio, Nat. Phys. **2**, 849 (2006); Phys. Rev. Lett. **99**, 160501 (2007); Laser and Photon Rev. **2**, No. 6, 527 (2008).
[20] A. D. Greentree, C. Tahan, J. H. Cole, and L. C. L. Hollenberg, Nat. Phys. **2**, 856 (2006).
[21] D. Rossini and R. Fazio, Phys. Rev. Lett. **99**, 186401 (2007).
[22] D. G. Angelakis, M. F. Santos, and S. Bose, Phys. Rev. A **76**, 031805(R) (2007).
[23] S. Bose, D. G. Angelakis, and D. Burgarth, J. Mod. Opt. **54**, 2307 (2007).
[24] D. G. Angelakis, M. F. Santos, V. Yannopapas, and A. Ekert, Phys. Lett. A. **362**, 377 (2007).
[25] M. X. Huo, Y. Li, Z. Song, and C. P. Sun, Phys. Rev. A **77**, 022103 (2008).
[26] L. Zhou, J. Lu, and C. P. Sun, Phys. Rev. A **76**, 012313 (2007).
[27] L. Zhou, H. Dong, Y. X. Liu, C. P. Sun, and F. Nori, Phys. Rev. A **78**, 063827 (2008).
[28] F. M. Hu, L. Zhou, T. Shi, and C. P. Sun, Phys. Rev. A **76**, 013819 (2007).
[29] L. Zhou, Y. B. Gao, Z. Song, and C. P. Sun, Phys. Rev. A **77**,

013831 (2008).
[30] T. Shi and C. P. Sun, Phys. Rev. B **79**, 205111 (2009).
[31] M. Wallquist, V. S. Shumeiko, and G. Wendin, Phys. Rev. B **74**, 224506 (2006).
[32] M. Sandberg, C. M. Wilson, F. Persson, T. Bauch, G. Johansson, V. Shumeiko, T. Duty, and P. Delsing, Appl. Phys. Lett. **92**, 203905 (2008).
[33] T. Yamamoto, K. Inomata, M. Watanabe, K. Matsuba, T. Miyazaki, W. D. Oliver, Y. Nakamura, and J. S. Tsai, Appl. Phys. Lett. **93**, 042510 (2008).
[34] M. A. Castellanos-Beltran, K. D. Irwin, G. C. Hilton, L. R. Vale, and K. W. Lehnert, Nat. Phys. **4**, 929 (2008).
[35] M. A. Castellanos-Beltran and K. W. Lehnert, Appl. Phys. Lett. **91**, 083509 (2007).
[36] A. Palacios-Laloy, F. Nguyen, F. Mallet, P. Bertet, D. Vion, and D. Esteve, J. Low Temp. Phys. **151**, 1034 (2008).
[37] J. R. Johansson, G. Johansson, C. M. Wilson, and F. Nori, Phys. Rev. Lett. **103**, 147003 (2009).
[38] N. Hatano, K. Sasada, H. Nakamura and T. Petrosky, Prog. Theor. Phys. **119**, 187 (2008).
[39] S. Data, *Quantum Transport: Atom to Transistor* (Cambridge University Press, Cambridge, 2005).
[40] O. Madelung, *Introduction to Solid State Theory* (Springer, Heidelberg, 1978).
[41] A. A. Houck, D. I. Schuster, J. M. Gambetta, J. A. Schreier, B. R. Johnson, J. M. Chow, and R. J. Schoelkopf, Nature (London) **449**, 328 (2007).